
PERGAMON

Available at
www.ElsevierComputerScience.com
POWERED BY SCIENCE DIRECT®

Pattern Recognition 38 (2005) 577–586

PATTERN RECOGNITION
THE JOURNAL OF THE PATTERN RECOGNITION SOCIETY
www.elsevier.com/locate/patcog

Classification and numbering of teeth in dental bitewing images☆

Mohammad H. Mahoor, Mohamed Abdel-Mottaleb*

Department of Electrical and Computer Engineering, University of Miami, 1251 Memorial Drive Coral Gables, FL 33146, USA

Received 20 May 2004; received in revised form 16 August 2004; accepted 16 August 2004

Abstract

We present an algorithm to classify and assign numbers to teeth in bitewing dental images. The goal is to use the result of this algorithm in an automated dental identification system. We use Bayesian classification to classify the teeth in a bitewing image into molars and premolars and assign an absolute number to each tooth based on the common numbering system used in dentistry. Fourier descriptors of the teeth contours are used as features in the Bayesian classification. After the Bayesian classification, the spatial relation between the two types of teeth is considered to number each tooth and correct the misclassification of some teeth in order to obtain high precision results. Comparison between the two kinds of FDs was done to select the best method for teeth classification. Experiments with 50 bitewing images containing more than 400 teeth show that our method is capable of classifying and assigning absolute index number to the teeth with high accuracy.

Keywords: Dental identification system; Forensic odontology; Bayesian classification; Fourier descriptors; Bitewing dental images

1. Introduction

Forensic radiology is part of forensic medicine, which is concerned with identifying people using postmortem radiological images of different parts of the body including skeleton, skull and teeth. The identification is carried out by comparing postmortem images with antemortem records of missing people to find similar records. Traditionally, dental based identification relies on information such as missing teeth and dental works [1–3]. Nowadays, with the advancements in dentistry and care of teeth by people, these methods might not be reliable; hence, developing new methods that use inherent dental features for identification is important [4–7].

Currently, we are designing and building an automated dental identification system (ADIS) for identification of people using dental X-ray images. This system is useful in the cases where other biometric methods for authentication i.e., fingerprint and iris are not applicable (e.g., fire victims). In order to build a fully automated system, we need to extract features from the teeth in the dental images of missing people and archive them in a database. During retrieval, the features for each tooth in the query image need to be extracted and compared to those stored in the database. If we limit the comparison of the teeth to the ones that have the same number, this will decrease the search space and increase the robustness of the system.

There are three types of dental radiographs, i.e. bitewing, panoramic, and periapical views. Bitewing images show molar and premolar teeth, periapical images provide a view of the front teeth, and panoramic images show all teeth in both jaws. Each of these views may be used to extract distinct features for identification [6]. In this work, we present

☆ This research is supported in part by the U.S. National Science Foundation under Award number EIA-0131079, the research is also supported under Award number 2001-RC-CX-K013 from the Office of Justice Programs, National Institute of Justice, U.S. Department of Justice.

* Corresponding author. Tel.: +1 305 284 3825; fax: +1 305 284 4044.
E-mail address: mottaleb@miami.edu (M. Abdel-Mottaleb).

0031-3203/$30.00
doi:10.1016/j.patcog.2004.08.012

an algorithm for the classification and numbering of the teeth in bitewing images based on their shapes.

In the literature, there are two categories for shape representation, i.e. contour based and region based [8,9] and each category has various methods with varying performance for different shapes. Brian Scassellati et al. [10] compared different shape description methods with human perceptual judgments. They evaluated shape similarity based on algebraic moments, spline curve distance, cumulative turning angle, sign of curvature and Hausdorff-distance with respect to human similarity judgments on twenty test shapes in a large image database. Moment invariants, which is in the category of region based, tended to work very well on objects where the distribution of the pixels, not the outline of the shape, was important. But on objects where the configuration of the outline was important, moments performed poorly. Basically, moments combine the information across an entire object rather than providing information just at a single boundary point. In our case, where we are only interested in distinguishing between molars and premolars, the outline of the teeth carry more information than the interior region. Therefore, we focus on the contour based approach for the representation of the teeth.

Fourier descriptors, FDs, are one of the most popular techniques for shape analysis and description in the category of contour based approach. Generally, it refers to a class of methods, not a single method, since there are many different ways in which the contour of a shape can be defined. A shape signature is any 1D representation of 2D areas or boundaries. The most common and practical shape signatures are the following: cumulative angular function, centroid distance, complex coordinates representation, and curvature signature. FDs were originally proposed by Cosgriff in 1960 [11] and thereafter became popular among the pattern recognition community through many works like [12–19]. These include using FDs for shape analysis [12], character recognition [13], shape coding [14], shape classification [15,16], and shape retrieval [17,18]. In biological sciences (biology, physical anthropology, etc.), Fourier descriptors of the contour have shown good results for classification of morphological forms such as plants, insects, fossils, and cells [19].

Zhang et al. [20] compared four different shape retrieval methods using Fourier descriptors with different shape signatures. They claim that shape retrieval using FDs derived from centroid distance signature is significantly better than that using FDs derived from complex coordinates, cumulative angular function, and curvature function. Shen et al. [21] claim that contour representation by complex coordinates is less sensitive to high-frequency noise and produces reliable results. Others [22] claim that by using elliptic Fourier descriptors, better results can be achieved. We prove in Appendix A that FDs derived from the complex coordinates signature has elliptic locus and in fact is a kind of elliptic Fourier descriptor. These reviews show that FDs derived from different signatures could have significant different effects on shape retrieval, but complex coordinates signature and centroid distance seems more powerful than the others. Hence, in this work we use Fourier descriptors based on complex coordinates signature and centroid distance for classification of the teeth.

This paper is organized as follows. Section 2 presents our method for dental classification. Section 3 discusses feature extraction and pre-classification of the teeth in bitewing images. Section 4 presents final classification and numbering of the teeth. Results of our method are presented in Section 5 and conclusions are in Section 6.

2. Method

2.1. Adult dentition system

The Adult dentition contains 32 teeth, 16 teeth in each jaw. We divide the two jaws into four equal quadrants that each quadrant contains eight teeth, two incisors, one cuspid (canine), two premolars (bicuspid), and three molars. As shown in Fig. 1, the numbering system numbers permanent teeth from 1 to 32, beginning at the maxillary right third molar (#1), extending across the maxilla to the left third molar (#16), then continuing to the left mandibular third molar (#17), and going around the mandibular arch to the right third molar (#32) [3]. Bitewing images usually contain two types of teeth, i.e., molar and premolar teeth. Sometimes part or whole of a cuspid tooth is visible in the image. The wisdom teeth, which have slightly different shapes from other molars, are sometimes missing or not visible in the bitewing images. In our work we consider the above information for final classification and numbering of molar and premolar teeth.

2.2. Dental classification method

Fig. 2 shows a block diagram as well as an annotated sample run of our method for the classification of molar and premolar teeth in bitewing images with the final numbering result. The method has three main steps: Teeth segmentation, Bayesian pre-classification using Fourier descriptors of each tooth contour, and final classification and numbering. The goal of the segmentation step is to obtain the contour of each individual tooth. We use the segmentation results

Right Maxilla								Left Maxilla							
1	2	3	4	5	6	7	8	9	10	11	12	13	14	15	16
32	31	30	29	28	27	26	25	24	23	22	21	20	19	18	17
Right Mandible								Left Mandible							

Fig. 1. The universal numbering system of adult teeth.

obtained from our two methods reported in Refs. [6,7]. The first method [6], performs enhancement of the original images by applying the top- and bottom-hat morphological operators. After obtaining an enhanced image, segmentation of teeth and background is done by adaptive thresholding to reduce the effect of noise and uneven intensity. In the second method [7], iterative thresholding followed by adaptive thresholding is used to segment teeth from background. After segmentation, integral projection is used to separate each tooth from its surroundings. Generally, in bitewing images, the crown of the teeth, either from the same jaw or from the two jaws may overlap. In such cases, integral projection properly separates the teeth. But in some images, the separation process may cause artifacts in the extracted contours of the teeth. Fig. 3 shows some results of applying integral projection for separating the teeth. Our algorithm is tolerant to these artifacts because it uses the first few coefficients of Fourier descriptors as will be explained in Section 3.

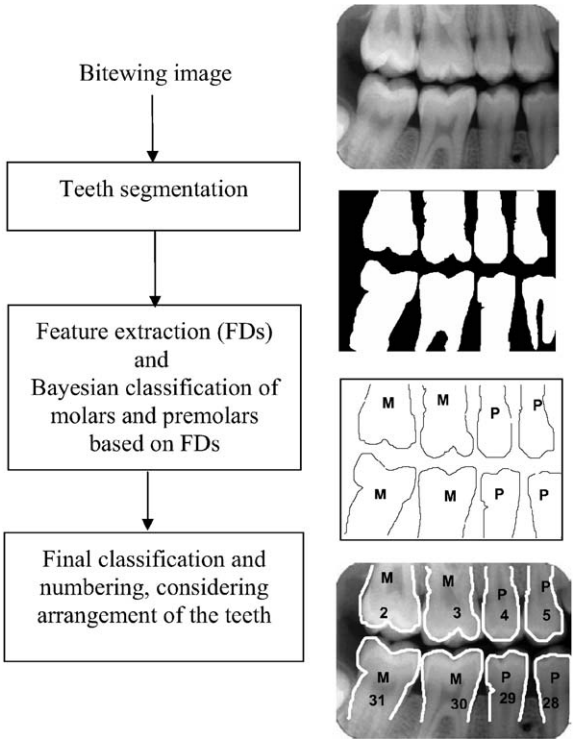

Fig. 2. Dental classification method diagram.

We used the results of these two segmentation methods by applying connected component analysis using 8-connectivity to extract the external contour of each individual tooth in the image. Fig. 4 shows some examples of applying these two methods for segmentation of bitewing images. We assume that the contours of the molars and premolars are open. Therefore the starting points are important for representation. The part of the teeth contour that we use for classification is the external boundary of crown and root. To normalize the number of contour points, there are generally three methods of normalization (i) equal points sampling, (ii) equal angle sampling and (iii) equal arc length sampling. In this work, we use equal points sampling for normalization of the teeth contour. Figs. 4c and d show examples of teeth contours which were used for feature extraction and classification.

3. Feature extraction and pre-classification

3.1. Complex coordinates signature

Fourier descriptors have useful properties including simplicity of implementation and concentration of the contour

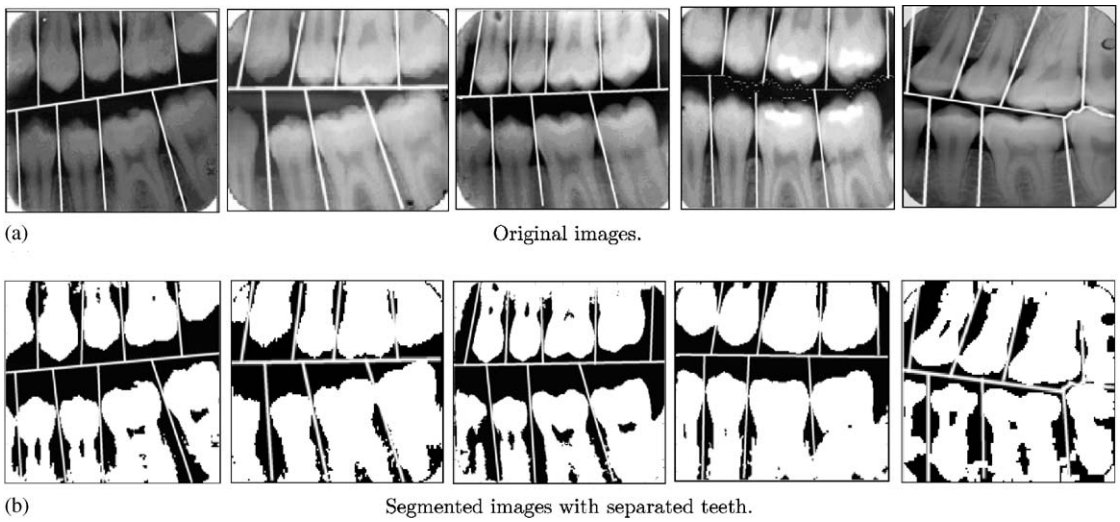

Fig. 3. Separating teeth using integral projection. (a) Original images. (b) Segmented images with separated teeth.

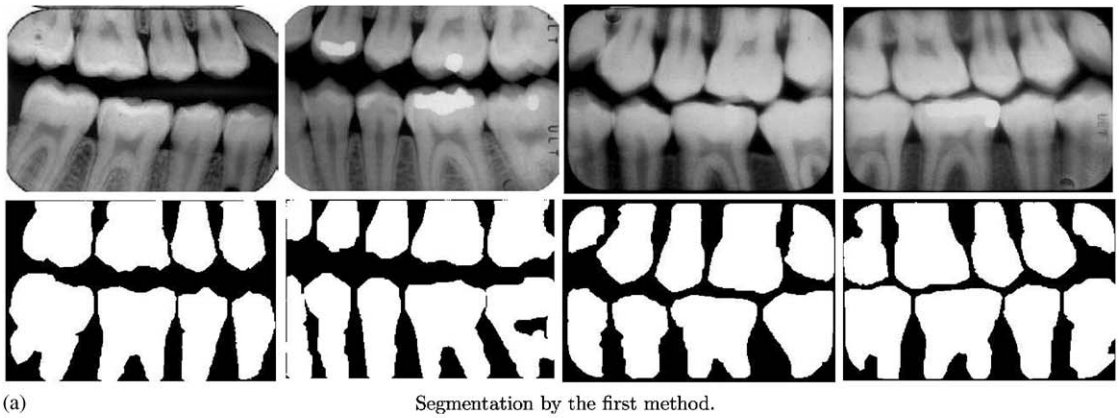

(a) Segmentation by the first method.

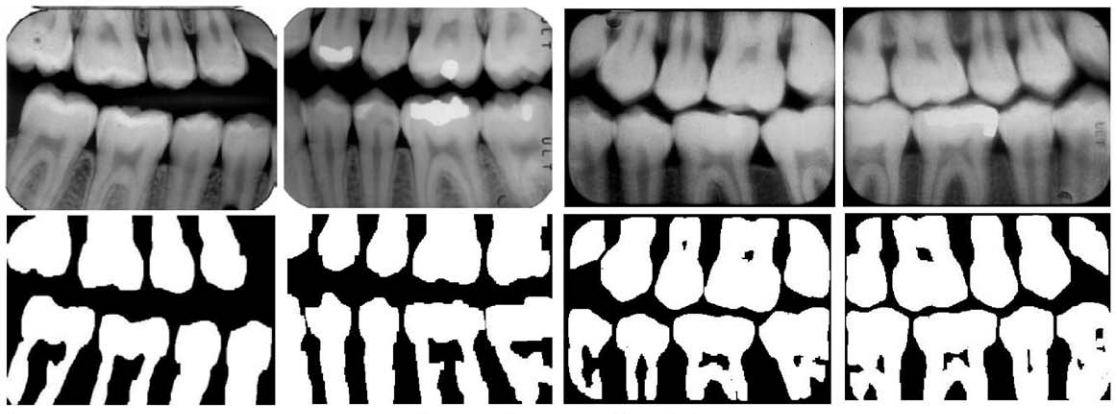

(b) Segmentation by second method.

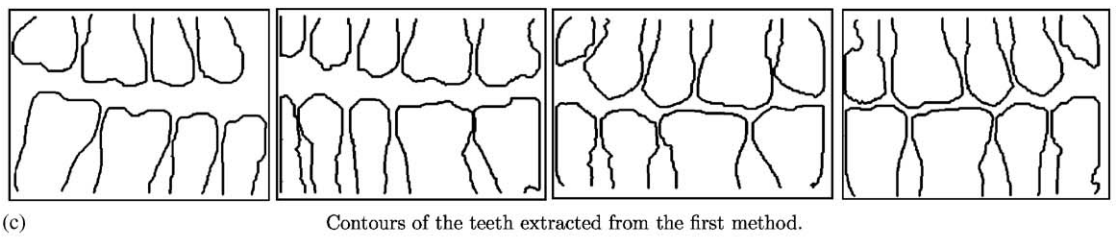

(c) Contours of the teeth extracted from the first method.

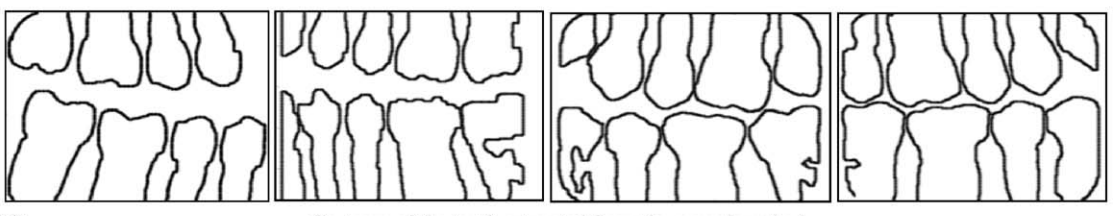

(d) Contours of the teeth extracted from the second method.

Fig. 4. Bitewing dental image segmentation. Original and segmented images. (a) Segmentation by the first method. (b) Segmentation by second method. (c) Contours of the teeth extracted from the first method. (d) Contours of the teeth extracted from the second method.

information in the first (low frequency) few coefficients [8]. We represent the contour of the teeth as a complex signal $u(n)$ defined based on the coordinates, $x(n)$ and $y(n)$, of the pixels that make the contour,

$$u(n) = x(n) + \mathrm{j}y(n). \tag{1}$$

We assume that this signal is periodic with period N, and then we apply Fourier transform to this complex signal,

$$U(s) = \frac{1}{N}\sum_{n=0}^{N-1} u(n)\mathrm{e}^{-(2\pi sn/N)}, \quad s = 0, 1, \ldots, N-1. \tag{2}$$

We use the Fourier coefficients, $u(s)$, to define a set of FDs, as shown in Eq. (3), that is invariant to translation, rotation and scaling.

$$f = \left[\frac{|U(2)|}{|U(1)|}, \frac{|U(3)|}{|U(1)|}, \ldots, \frac{|U(N-1)|}{|U(1)|}\right]. \tag{3}$$

Translation invariance is achieved by discarding the first coefficient ($s = 0$), scale invariance is brought by dividing the other coefficients by the second coefficient ($s = 1$), and rotation invariance is achieved by using only absolute values of the coefficients. In the cases where the contour of the shape is closed, effect of starting point is canceled by using only absolute values, although in our case the contour is open but we start from the same starting point for each contour. The first few coefficients of feature vector in Eq. (3) were used for Bayesian classification.

3.2. Centroid distance

The centroid distance function is expressed by the distance of the boundary points from the centroid (x_c, y_c) of the shape, which is invariant to translation,

$$x_c = \frac{1}{N}\sum_{n=0}^{N-1} x(n), \tag{4}$$

$$y_c = \frac{1}{N}\sum_{n=0}^{N-1} y(n), \tag{5}$$

$$r(n) = ([x(n) - x_c]^2 + [y(n) - y_c]^2)^{1/2} \tag{6}$$

we assume the signal $r(n)$ is periodic with period N, and we apply Fourier transformation on this real signal. Because the signal is real, there are only $N/2$ different frequencies in the result of Fourier transformation (magnitude of the frequency response is symmetric) and we define the feature vectors to consist of the coefficients corresponding to the low frequency components. Scale invariance is obtained by dividing the magnitude values of the FDs coefficients by the DC component ($s = 0$), rotation invariance is achieved by taking only the magnitude values of the FDs. The invariant feature vector used to describe the shape by centroid distance consists of the first few coefficients in the following vector,

$$f = \left[\frac{|U(1)|}{|U(0)|}, \frac{|U(2)|}{|U(0)|}, \ldots, \frac{|U(N/2)|}{|U(0)|}\right]. \tag{7}$$

3.3. Bayesian classification of teeth

Let c_i denote tooth class i, i.e., molar or premolar, and x denotes the feature vector, complex coordinates signature or centroid distance. Suppose that we know the prior probabilities $p(c_i)$ and the conditional densities $p(x|c_i)$. Bayes rule shows how observing the value of x changes the prior probability $p(c_i)$ to a posteriori probability $p(c_i|x)$ [23],

$$p(c_i|x) = \frac{p(x|c_i)p(c_i)}{p(x)}, \tag{8}$$

where $p(x) = \sum_{i=1}^{C} p(x|c_i)p(c_i)$ and C is number of classes.

In order to obtain a posteriori probability we need to estimate $p(x|c_i)$ and $p(c_i)$. We assume that our feature vectors have a Gaussian distribution, therefore $p(x|c_i)$ can be defined as

$$p(x|c_i) = \frac{1}{(2\pi)^{d/2}|\Sigma_i|^{1/2}} \times \exp\left[-\frac{1}{2}(x-\mu_i)^t \Sigma_i^{-1}(x-\mu_i)\right], \tag{9}$$

where μ_i is the mean vector, Σ_i is the covariance matrix, and d is the dimension of the Gaussian distribution. We use Eqs. (10) and (11) to estimate the mean vector μ_i and the covariance matrix Σ_i for class c_i,

$$\mu_i = \frac{1}{N_i}\sum_{j=1}^{N_i} x_{i,j} \tag{10}$$

$$\Sigma_i = \frac{1}{N_i - 1}\sum_{j=1}^{N_i} (x_{i,j} - \mu_i)(x_{i,j} - \mu_i)^t \tag{11}$$

where N_i is the number of observations in class i.

For maximum a posteriori classification, we choose class c_i which maximizes Eq. (8) and we define a decision function as the logarithm of $p(c_i|x)$. Since $p(x)$ is constant, we ignore it; therefore the decision function has the form

$$g_i(x) = \ln(p(x|c_i)) + \ln(p(c_i)) \tag{12}$$

This means that a feature vector, x, is classified as belonging class c_i, if the condition in Eq. (13) is satisfied.

$$g_i(x) > g_j(x) \quad \text{for all } i \neq j \tag{13}$$

where $i, j \in \{1, 2, \ldots, C\}$. We define two sets of classes for the lower and the upper jaws. We have two classes for the molar and the premolar teeth of the mandible and two other classes for the molar and the premolar teeth of the maxilla. Because we deal with the upper and lower jaws separately, we have two classes for each jaw, and the decision function for each jaw has the form,

$$g(x) = g_1(x) - g_2(x) \tag{14}$$

if $g(x)$ is positive, then we assign the feature vector x to class c_1 (Molar), otherwise to class c_2 (Premolar). The value

of $g_i(x)$ is considered as a confidence measure. The large values of that measure signal robust decisions. These confidence measures are used for the correction of the misclassification in the final classification and numbering.

4. Final classification and numbering

Fig. 5 shows the arrangement of the molar and the premolar teeth in the bitewing images of the left and the right quadrants. We assume that the images are not flipped vertically; therefore, molar teeth are in the left most side of the image for radiographs of the right quadrant, and in the right most side of the image for radiographs of the left quadrant. There is one molar adjacent to a premolar in each quadrant, and above each mandibular molar (or premolar), there is a maxillary molar (or premolar).

During classification, we need to deal with the difficulties arising from missing part of the teeth at the border of the bitewing images. In addition, some images contain cuspid teeth, which are mostly like premolar teeth, and distinguishing them needs more consideration. Wisdom teeth, which are members of the molar teeth, are different in shape compared to the other molar teeth. To resolve these problems, the spatial relations between the teeth in bitewing images are considered. By using this information, after the classification of the teeth into molars and premolars, we correct misclassifications and assign a number to each individual tooth. For correcting the misclassification, we follow this algorithm:

We search for the tooth with a confidence measure less than a threshold. If the confidence measure of the tooth above/below is greater than it and their class membership are different, then we consider the tooth with low confidence measure as a misclassified tooth and assign it to the same class as the tooth with high confidence measure. Otherwise, if the two teeth have the same classification, we do not change the class membership. This operation will be repeated for all teeth in mandible and maxilla. In the next step, we check the arrangement of the teeth in each jaw. The teeth arrangement without missing tooth should match one of these patterns:

PM, PMM, PMMM, PPM, PPMM and PPMMM (left quadrant image)

MP, MMP, MMMP, MPP, MMPP and MMMPP (right quadrant image)

We discard the cases with only molar or premolar teeth such as M, MM, MMM, P and PP. In fact, without both premolar and molar teeth in the image, it is not possible to assign a number to each tooth.

5. Experiments and results

Fig. 4 shows results of the segmentation of the teeth in the bitewing images using the two different algorithms. The first method is more efficient than the second one, which needed some manual correction for the segmented images. After segmentation, we extract the contour of each tooth in the binary image by applying connected component analysis. We used 25 bitewing images as a training set to estimate the prior distribution $p(c_i)$ and the conditional distribution $p(x|c_i)$. Eqs. (10) and (11) were used to estimate the mean and the covariance for each class. For classification, 50 images, different from the training set, containing 220 molar and 180 premolar teeth were randomly selected and segmented. Then, we used the Bayesian classification method to preclassify the teeth. Tables 1 and 2 show the results of pre-classification using the different segmentation algorithms. The results show that complex coordinate signature is slightly powerful than the centroid distance for classification of the teeth. But for some images that are segmented by the second method, like premolars in maxilla, the centroid distance provided better results. Tables 3 show the results of the final classification with the consideration of the arrangement of the teeth. The results show a considerable change in performance. The most change is in the performance of the premolars in maxilla with a factor of 18% from 72.0% to 94.2%. Our experiments show that the classification of premolars is more difficult than molars for both jaws. For maxillary teeth, the shape of the root is not as visible as in case of the mandibular teeth and this

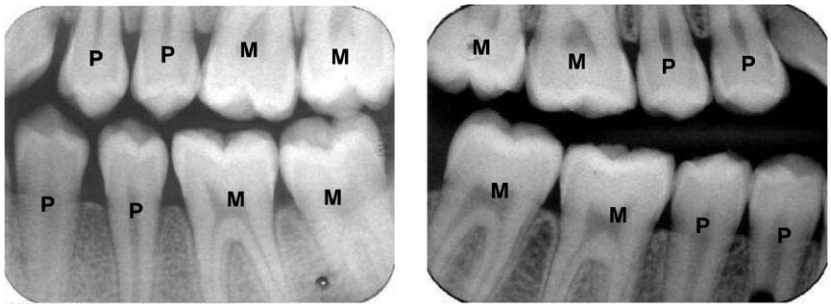

Fig. 5. Arrangement of teeth in dental bitewing images. (a) left quadrant and (b) right quadrant, M: Molar, P: Premolar.

Table 1
Pre-Classification of teeth using first method of segmentation

Teeth	Performance ratio % (complex signature)	Performance ratio % (centroid distance)
Molars in Mandible	95.5	95.5
Premolars in Mandible	86.4	81.5
Molars in maxilla	83.7	86.4
Premolars in Maxilla	86.4	72.0

Table 2
Pre-Classification of teeth using second method of segmentation

Teeth	Performance ratio % (complex signature)	Performance ratio % (centroid distance)
Molars in Mandible	89.7	89.3
Premolars in Mandible	82.7	78.7
Molars in maxilla	91.4	86.4
Premolars in Maxilla	72.0	80.0

Table 3
Final classification of teeth using first method of segmentation

Teeth	Performance ratio % (complex signature)	Performance ratio % (centroid distance)
Molars in Mandible	95.5	95.5
Premolars in Mandible	86.4	84.2
Molars in maxilla	93.7	95.5
Premolars in Maxilla	92.0	90.0

Table 4
Final classification of teeth using second method of segmentation

Teeth	Performance ratio % (complex signature)	Performance ratio % (centroid distance)
Molars in Mandible	91.8	91.4
Premolars in Mandible	91.4	85.1
Molars in maxilla	93.7	91.4
Premolars in Maxilla	82.0	94.2

makes the classification more difficult for maxillary teeth. For mandibular teeth the crowns of premolar teeth in some cases are similar to the crowns of molar teeth. Molar teeth in mandible jaw have at least two roots and both roots are visible in bitewing images, but molar teeth in maxilla have three or four roots which are projected on each other in bitewing images. Fig. 6 and 4 shows the results of final classification and numbering of the teeth in some bitewing images that we used in our experiments.

Fig. 7 shows some difficult cases, where classification and numbering did not give good results. We can notice in Fig. 7a that there are missing teeth. Although, the classification is correct, the numbering of the teeth is not correct. In Fig. 7b, we can see some images with misclassification. In these cases, the roots of the teeth in images are not completely visible and it makes classification difficult.

The classification of the teeth in the border of the images is difficult because parts of the teeth are not visible in the image, but they can be correctly classified by using the information about the neighboring teeth.

6. Conclusions

We introduced a method for robust classification and numbering of molar and premolar teeth in bitewing images using Bayesian classification. Two different kinds of Fourier descriptors, i.e., complex coordinates signatures and centroid distance of the contours, were used for feature description and classification. After classification, our algorithm considers the arrangement of the teeth in the jaw to correct any misclassifications and to assign a number to each tooth based on common numbering system of dentistry. In this paper, we did not consider the case of missing teeth. The algorithm for molar and premolar classification (not numbering) can still work for cases with missing teeth. To obtain correct numbering of the teeth, we are developing an algorithm for detecting missing teeth.

Appendix A.

In this section, we prove that FDs of the 1D sequence of complex coordinates also has elliptic locus and there are no differences between the elliptic Fourier descriptors and 1D complex coordinates FDs. In Section A.1, we review the parametric equations of an ellipse curve and prove the relation between these equations in different forms. Then in Section A.2, we use the parametric equation of the ellipse in complex coordinates to prove that FDs of the 1D complex coordinates have elliptic locus.

A.1. Parametric equations of an ellipse curve

An ellipse is the locus of the points in a plane such that the summation of their distances from two fixed points, which called focus are constant. In other words, ellipse is a conical section with eccentricity greater than zero and less than one. As shown in Fig. 8, ellipse has two axes, major and minor with foci on the major axis. There are many ways to represent the points on an ellipse. In general form, Eq. (A.1) represents an ellipse which is not centered on the origin of the Cartesian coordinates and also the major and minor axes are not parallel to x and y axes.

$$Ax^2 + By^2 + 2Hxy + Cx + Dy + E = 0. \quad \text{(A.1)}$$

Fig. 6. Classification and numbering of the teeth in dental bitewing images. (a) Right jaw. (b) Left jaw.

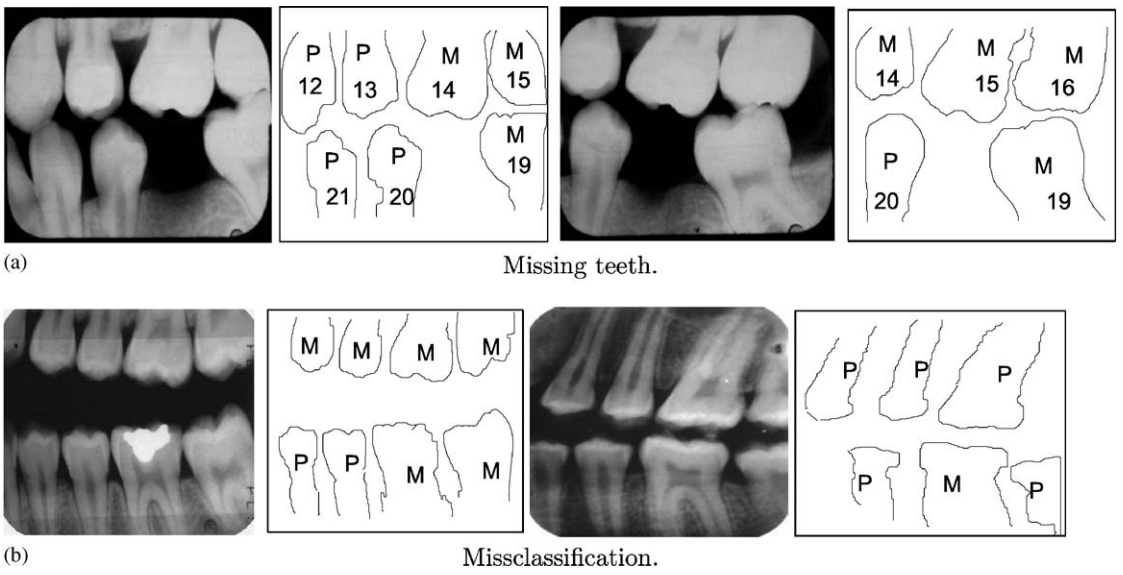

Fig. 7. Difficult cases for numbering and classification. (a) Missing teeth. (b) Missclassification.

For the simple case of Fig. 8 where major and minor axes are parallel to coordinate axes x and y, and the centroid of the ellipse curve is on the origin, Eq. (A.1) has the simple form,

$$\frac{x^2}{a^2} + \frac{y^2}{b^2} = 1 \quad \text{where } a^2 - c^2 = b^2. \tag{A.2}$$

General parametric equation for an ellipse curve are as following.

$$x = a\cos\theta + b\sin\theta, \quad y = c\cos\theta + \mathrm{d}\sin\theta, \tag{A.3}$$

$$Z = A\exp(\mathrm{j}\theta) + B\exp(-\mathrm{j}\theta), \tag{A.4}$$

where $0 \leqslant \theta \leqslant \pi$ and a, b, c and $d \in R$, A *and* $B \in Z$.

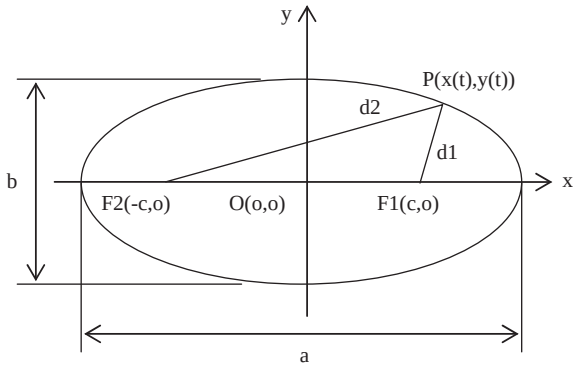

Fig. 8. Ellipse curve.

Each of these two representations can be proved to be locus of an ellipse as follows:

Consider the ellipse of Fig. 8 with parametric equation $x = a_1 \cos\theta$, $y = b_1 \sin\theta$, under rotation by angle α, we get,

$$\begin{bmatrix} x' \\ y' \end{bmatrix} = \begin{bmatrix} \cos\alpha & \sin\alpha \\ -\sin\alpha & \cos\alpha \end{bmatrix} \begin{bmatrix} a_1 \cos\theta \\ b_1 \sin\theta \end{bmatrix} \quad (A.5)$$

therefore,

$$x' = a_1 \cos\alpha \cos\theta + b_1 \sin\alpha \sin\theta = a \cos\theta + b \sin\theta,$$

and

$$y' = -a_1 \cos\alpha \sin\theta + b_1 \sin\alpha \cos\theta = c \cos\theta + \mathrm{d} \sin\theta$$

This is the same representation as in Eq. (A.3).

For Eq. (A.4), if we express the complex numbers A and B in polar forms,

$Z = r_1 \exp(\mathrm{j}\alpha_1 + \mathrm{j}\theta) + r_2 \exp(\mathrm{j}\alpha_2 - \mathrm{j}\theta)$ then by using the Euler formula, we would have,

$Z = [r_1 \cos(\theta+\alpha_1) + r_2 \cos(\theta-\alpha_2)] + \mathrm{j}[r_1 \sin(\theta+\alpha_1) - r_2 \sin(\theta-\alpha_2)]$

we know that the summation of two sinusoids is also a sinusoid, therefore, this complex number can be rewritten as,

$Z = R_1 \cos(\theta+\theta_1) + \mathrm{j}R_2 \sin(\theta+\theta_2)$ which is the parametric equation of an ellipse with its axes not parallel to the coordinates axes.

A.2. Elliptic fourier descriptor

The elliptic Fourier descriptor is the series expansion of the boundary coordinates of a closed contour $x(t)$ and $y(t)$,

$$x(t) = A_0 + \sum_{n=1}^{\infty} \left[a_n \cos\frac{2\pi nt}{T} + b_n \sin\frac{2\pi nt}{T} \right], \quad (A.6)$$

$$y(t) = C_0 + \sum_{n=1}^{\infty} \left[c_n \cos\frac{2\pi nt}{T} + d_n \sin\frac{2\pi nt}{T} \right]. \quad (A.7)$$

It was proved by Kuhl and Giardina [22] that all of the components in the summation have elliptic loci. They proposed a method for deriving the Fourier coefficients corresponding to nth harmonics a_n, b_n, c_n, and d_n. The derivation of the coefficients involves the Fourier representation of the time derivative $\dot{x}(t)$ and $\dot{y}(t)$ and equating them with direct derivative of the Fourier series of signal $x(t)$ and $y(t)$.

Now we focus on complex coordinates signature. We can represent the periodic discrete boundary signal $u(n) = x(n) + \mathrm{j}y(n)$, using the discrete Fourier transform,

$$u(n) = C_0 + \sum_{k=1}^{N/2} \left[C_k \exp\frac{-\mathrm{j}2\pi nk}{N} + C_{-k} \exp\frac{\mathrm{j}2\pi nk}{N} \right] \quad (A.8)$$

where $n = 0, 1, \ldots, N-1$. Coefficients C_k and C_{-k} with complex values are the FDs of the contour. We consider that the coefficients C_k and C_{-k} are not complex conjugate symmetric or no other symmetric relationship between them. The term under summation of Eq. (A.8) has the form $Z = A \exp(\mathrm{j}\theta) + B \exp(-\mathrm{j}\theta)$ and this proves that it has elliptic locus. Therefore 1D sequence of complex coordinates is the summation of points with elliptic loci. The coefficients of EFDs can be related to complex coordinates Fourier descriptors as follows:

$$a_k = \frac{1}{2} Re\{C_k + C_{-k}\}, \quad b_k = \frac{1}{2} Im\{C_n - C - n\}, \quad (A.9)$$

$$c_k = \frac{1}{2} Re\{C_k - C_{-k}\}, \quad d_k = \frac{1}{2} Im\{C_n + C - n\}. \quad (A.10)$$

To compute the coefficients of EFDs, it is convenient to use Eqs. (A.9) and (A.10) rather than using the previous one.

References

[1] United States Army Institute of Dental Research Walter Reed Army Medical Center, Computer assisted post mortem identification via dental and other characteristics, USAIDR Inf. Bull. 5(1).
[2] American society of forensic odontology, Forensic Odontol. News 16(2).
[3] B.G. Brogdon, Forensic Radiology, CRC Press, Boca Raton, 1998.
[4] A. Jain, L. Hong, S. Pankanti, Biometric identification, Commun. ACM 43 (2) (2000) 91–98.
[5] S. Pankanti, R. Bolle, A. Jain, Biometric: the future of identification, IEEE Comput. (2000) 46–49.
[6] J.D. Zhou, M. Abdel-Mottaleb, Automatic human identification based on dental X-ray images, in: Proceedings of the SPIE Conference on Defense and Security—Biometric Technology for human Identification, 2004.
[7] M. Abdel-Mottaleb, O. Nomir, D.E. Nasser, G. Fahmy, H.H. Ammar, Challenges of developing an automated dental identification system, in: The 64th IEEE Midwest Symposium on Circuits and Systems, Cairo, Egypt, 2003.

[8] L.F. Costa, R.M. Cesar, Shape Analysis and Classification: Theory and Practice, CRC Press, Boca Raton, FL, 2000.
[9] D. Zhang, G. Lu, An integrated approach to shape based image retrieval, The Fifth Asian Conference on Computer Vision, ACCV, 2002, pp. 652–657.
[10] B. Scassellati, S. Alexopoulos, M. Flickner, Retrieving images by 2d shape: a comparison of computation methods with human perceptual judgments, SPIE 2185 (1994) 2–14.
[11] R.L. Cosgriff, Identification of Shape, Ohio State University Research Foundation, Columbus, Report 820-11 ASTIA AD 254 792, 1960.
[12] P.J. van Otterloo, A contour-Oriented Approach to Shape Analysis, Prentice-Hall, UK, 1991.
[13] E. Persoon, K.S. Fu, Shape discrimination using fourier descriptors, IEEE Trans. Syst. Man Cybern. 7 (3) (1977) 170–179.
[14] R. Chellappa, R. Bagdazian, Fourier coding of image boundaries, IEEE Trans. PAMI 6 (1) (1984) 102–105.
[15] H. Kauppinen, T. Seppanen, M. Pietikainen, An experimental comparison of autoregressive and fourier-based descriptors in 2d shape classification, IEEE Trans. PAMI 17 (2) (1995) 201–207.
[16] C.T. Zahn, R.Z. Roskies, Fourier descriptors for plane closed curves, IEEE Trans. Comput. 21 (3) (1972) 269–281.
[17] C.L. Huang, D.H. Huang, A content-based image retrieval system, Image Vision Comput. 16 (1998) 149–163.
[18] G. Lu, A. Sajjanhar, Region-based shape representation and similarity measure suitable for content-base image retrieval, Multimedia Syst. 7 (1999) 165–174.
[19] P.E. Lestrel, Fourier Descriptors and Their Applications in Biology, Cambridge University Press, USA, 1997.
[20] D. Zhang, G. Lu, A comparative study on shape retrieval using fourier descriptors with different shape signatures, in: Proceedings of International Conference on Intelligent Multimedia and Distance Education (ICIMADE01), 2001, pp. 1–9.
[21] L. Shen, R.M. Rangayyan, J.E.L. Desaultes, Application of shape analysis to mammographic classifications, IEEE Trans. Med. Imag. 13 (1994) 263–274.
[22] P. Kuhl, C. Giardina, Elliptic fourier features of a closed contour, CGIP 18 (1982) 236–258.
[23] R.O. Duda, P.E. Hart, Pattern Classification and Scene Analysis, Wiley, New York, 2000.